nkx3.2 mutant zebrafish accommodate the jaw joint loss through a phenocopy of the head shapes of Paleozoic agnathans

Tetsuto Miyashita[1, 2], Pranidhi Baddam[3], Joanna Smeeton[4], A. Phil Oel[1, 5], Natasha Natarajan[4], Brogan Gordon[1], A. Richard Palmer[1], J. Gage Crump[4], Daniel Graf[3, 6], and W. Ted Allison[1, 6]*

[1] Department of Biological Sciences, University of Alberta, Edmonton, Alberta, Canada T6G 2E9

[2] Department of Organismal Biology and Anatomy, University of Chicago, Chicago, IL 60637, USA

[3] Department of Dentistry, University of Alberta, Edmonton, Alberta, Canada T6G 2R3

[4] Department of Stem Cell Biology and Regenerative Medicine, W.M. Keck School of Medicine, University of Southern California, Los Angeles, CA 90033, USA

[5] Current Address: Developmental Biology Unit, European Molecular Biology Laboratory, Heidelberg, 69117, Germany

[6] Department of Medical Genetics, University of Alberta, Edmonton, Alberta, Canada T6G 2R7

* Corresponding author. ted.allison@ualberta.ca; 780-492-4430.

Abstract

The vertebrate jaw is a versatile feeding apparatus that facilitated explosive diversification. Its functions require a joint between the upper and lower jaws, so jaw joint defects — such as osteoarthritis or even ankylosis — are often highly disruptive and difficult to study. To describe consequences of jaw joint dysfunction, we engineered two independent null alleles of a single jaw-joint marker gene, *nkx3.2*, in zebrafish. The mutations caused the fish to become functionally jawless via a fusion between the upper and lower jaw cartilages (ankylosis). Surviving to adulthood despite lacking jaw joints, *nkx3.2* mutants accommodate this defect by: a) remodeling their skulls drastically from juvenile to adult stages; and b) altering their feeding behaviors from suction to ram feeding. As a result of the remodeling, *nkx3.2* mutants developed superficial similarities to the skull shapes observed in two lineages of ancient jawless vertebrates (anaspids and furcacaudiform thelodonts), including: a fixed open gape, reduced snout, and enlarged branchial region. However, no homology exists in individual skull elements between these taxa, and most of the modified elements in the mutant zebrafish occur outside known expression domains of *nkx3.2*. Therefore, we interpret the adult *nkx3.2* phenotype not as a reversal to an ancestral state, but as convergence due to similar functional requirement of feeding without mobile jaws. This remarkable convergence underscores jaw joint functions as a powerful constraint during the development of jawed vertebrate skulls, which implies that functionally viable morphological patterns are finite, with or without functional jaws. Because *nkx3.2* null zebrafish display prominent joint ankylosis, drastically modified skull shape, and altered feeding behaviors, these mutants provide a unique model with which to investigate mechanisms of skeletal remodeling and joint diseases.

Introduction

The jaw is a functionally versatile innovation that facilitated explosive diversification of gnathostomes (a clade containing jawed vertebrates), but its basic structure is surprisingly simple and highly

27 conservative (Miyashita, 2016). A jaw consists of 'a hinge and caps': an upper and lower skeletal
28 levers hinged at a jaw joint (Depew and Simpson, 2006). As the joint enables biting motions, its origin
29 is considered the final step in the evolutionary assembly of the vertebrate jaws (Cerny et al., 2010;
30 Kuratani, 2012; Miyashita, 2016). Across jawed vertebrates, the presumptive jaw joint is marked by the
31 expression of *nkx3.2*, an NK2 class homeobox gene (a.k.a. *bapx*), at the midheight of the embryonic
32 mandibular arch (Gillis et al., 2013; Lukas and Olsson, 2018a; Miller et al., 2003; Tucker et al., 2004).
33 Chondrogenesis dorsal to this expression domain gives rise to a palatoquadrate (upper jaw), whereas
34 chondrogenesis ventral to it forms Meckel's cartilage (lower jaw) (Medeiros and Crump, 2012). This
35 basic pattern remains conserved among jawed vertebrates, but later development varies. Marginal
36 bones arise intramembranously around the often endo-/perichondrally ossified jaw cartilages except in
37 chondrichthyans (sharks, rays, and skates) (Hall, 2015). In mammals, the jaw joint instead forms
38 between two such intramembranous bones (temporal and dentary), whereas the proximal jaw joint
39 becomes the malleus-incus interface that is, in mice, no longer affected by *Nkx3.2* knockout (Tucker et
40 al., 2004). Despite these variations after pharyngeal chondrogenesis, no gnathostome lineage
41 secondarily lost functional jaws.

42 By studying functional jaw loss in our new mutant zebrafish, we asked whether — and how —
43 jaw functions affect the vertebrate skull shape during development. Clinically documented agnathia in
44 humans typically accompanies severe congenital disorders such as holoprosencephaly and otocephaly,
45 but the jaw loss is clearly a secondary effect and not a cause in these cases (Bixler et al., 1985; Brown
46 and Marsh, 1990; Gekas et al., 2010; Schiffer et al., 2002). Instances of temporomandibular joint
47 ankylosis may result from trauma or infection, or may be congenital (Adekeye, 1983; Chidzonga, 1999;
48 Manganello-Souza and Mariani, 2003). If untreated, the ankylosis can lead to the 'bird face' deformity
49 (El-Sheikh et al., 1996). However, these cases do not fully document the effects of functional jaw loss.
50 In mammalian models, various jaw/skull deformations have been induced by surgical resection,
51 detachment, or repositioning of the jaw muscles and/or bones (Bayram et al., 2010; Gomes et al., 2012;

52 Horowitz and Shapiro, 1955; Lifshitz, 1976; Miyazaki et al., 2016; Rodrigues et al., 2009; Sarnat,
53 1970; Sarnat and Muchnic, 1971; Toledo et al., 2014). These manipulations occurred well after the
54 formation of the jaw skeleton and muscles, and the jaws remained partially functional because of
55 unilateral operations or non-comprehensive disruption. The defects and deformities reported in these
56 studies imply: a) jaw functions are potentially an important factor in shaping the skulls; and b) any
57 allele disrupting jaw functions would be generally maladaptive. Nevertheless, these implications are
58 difficult to explore in the absence of an accessible experimental model.

59 To fill in this gap, we engineered two distinct null alleles of *nkx3.2* in zebrafish. Previously,
60 transient knockdown of *nkx3.2* during early development (using morpholinos) had shown fusion of the
61 nascent jaw cartilages in both zebrafish and frogs (Lukas and Olsson, 2018a; Miller et al., 2003). We
62 confirmed in zebrafish that the mutants recapitulate this phenotype. Surprisingly, mutant zebrafish are
63 viable despite the loss of the jaw joint persisting through adulthood. Thus functionally jawless, *nkx3.2*$^{-/-}$
64 zebrafish dramatically alter the skull shapes late in ontogeny to facilitate feeding, with the mouth fixed
65 open, the snout reduced, and the branchial region expanded. This open-mouth phenotype, previously
66 unknown in zebrafish or in other jawed vertebrates, also occurred in two extinct lineages of 400-
67 million-plus year-old jawless vertebrates, anaspids and thelodonts. Even though they share no
68 homology in individual facial bones, the *nkx3.2*$^{-/-}$ fish accommodate functional jaw loss by converging
69 onto these ancient, distantly related agnathans in overall head shapes. Thus, *nkx3.2* mutant zebrafish
70 provide a unique model for both skeletal remodeling and joint diseases such as osteoarthritis, and to
71 reevaluate evolutionary implications of phenocopies in general.

72

73 **Methods**

74 Full methodological details are available in Supplementary Information.

75

76 **Animal Ethics.** Zebrafish maintenance and experiments were approved as protocol number

77 AUP00000077 by the Animal Care and Use Committee: Biosciences at the University of Alberta as
78 dictated by the Canadian Council on Animal Care. Other zebrafish work was approved by the
79 University of Southern California Institutional Animal Care and Use Committee.
80
81 **Molecular genetics.** Two disparate regions of the gene were targeted by CRISPR guide RNA (gRNA)
82 or TALENs, producing two disparate null alleles that produced similar phenotypes (Fig. 1a). One allele
83 (ua5011) was engineered with CRISPR/Cas9 (Gagnon et al., 2014) targeted at the beginning of the
84 homeodomain, and it harbors a 20 bp deletion resulting in a frameshift (Fig. 1a; Data Supplement 1).
85 The disrupted translation of codons is predicted to abrogate production of the critical homeobox
86 domain, and instead produce random amino acids. This is predicted to produce a non-functional
87 Nkx3.2 and a null allele. A disparate allele (el802) was generated using TALENs (Barske et al., 2016)
88 targeted at the start of the gene. This produced a stably inherited gene with 20 bp deletion, removing
89 the translation start codon (Fig. 1a). The allele *nkx3.2*^{el802} is predicted to not produce Nkx3.2 protein.
90 Morphologically, these two alleles are not readily distinguishable from each other (see Results).
91
92 **Morphometrics.** We compared gapes in zebrafish and anaspids (a lineage of extinct jawless
93 vertebrates) (Blom et al., 2001) by taking the angle between skeletal elements of the upper and lower
94 lips (Data Supplement 2). In zebrafish, the angle was taken by extrapolating the axis of the premaxilla
95 until it meets the axis of the dentary. At younger stages (4 and 14 dpfs), the angle was measured
96 between the axes of the palatal process and Meckel's cartilage. In anaspids, the upper and lower lips
97 are demarcated by a series of relatively larger scales, which allowed delineation of the gape angle
98 (measured at where the extrapolated upper and lower lip margins meet). For geometric morphometric
99 comparison, eight landmarks were assigned to both zebrafish (2 mpf) and anaspid samples to capture
100 overall head shapes (see Supplementary Information for rationales of landmark assignment). From the
101 pool of nearly a thousand catalogued specimens of anaspids, we selected a total of 70 specimens that

show lateral compression during the fossilization process, with the least taphonomic artifact, to reflect lateral view of the heads. Furcacaudiform thelodonts were excluded because only a handful of exceptionally preserved specimens are available. The sample size is small for this latter group, and all such specimens were collected from a single locality, making it difficult to control for taphonomic artifacts. The landmark data (Data Supplement 2) were transformed using the Procrustes superimposition method (Rohlf, 1999), and the resulting coordinates were compared using Principal Component Analysis (PCA).

Results

Jaw joint is ankylosed in *nkx3.2* null alleles

At 4 days post fertilization (dpf), *nkx3.2*$^{-/-}$ zebrafish replicate the *nkx3.2* morpholino knockdown phenotype: the absence of a jaw joint (Miller et al., 2003). The palatoquadrate and Meckel's cartilage are fused to each other, and the retroarticular process is absent (Fig. 1d, g, i). Apart from the joint ankylosis, no marked differences exist in body profile, overall size, or survival rates between *nkx3.2*$^{-/-}$ mutants and wildtype. Heterozygotes are morphologically indistinguishable from wildtype (Fig. 1c, f), and the *nkx3.2* alleles display recessive Mendelian inheritance. Remarkably, these functionally jawless homozygous mutants survive beyond early larval stages.

Functionally jawless *nkx3.2*$^{-/-}$ zebrafish modify skull shapes late in ontogeny

Counterintuitive to the maladaptive nature of jaw dysfunctions in general, *nkx3.2*$^{-/-}$ zebrafish continue to grow without a jaw joint. Marked phenotypic differences against wildtype begin to emerge between the 2nd and 3rd weeks post fertilization (Fig. 2). The lower jaw becomes downturned in *nkx3.2*$^{-/-}$ fish resulting in a rigidly fixed open mouth, whereas both upper and lower jaws are upturned in wildtype zebrafish (Fig. 2a, b). This coincides with the onset of ossification and the period of active feeding in

127 normal juveniles (Cubbage and Mabee, 1996; Kimmel et al., 1995). Although the palatoquadrate and
128 Meckel's cartilage remain fused in *nkx3.2*$^{-/-}$ mutants, skeletal staining reveals that the upper and lower
129 jaw elements ossify independently of each other — still without a ball-and-socket joint structure (Fig.
130 2k, l). All skull elements ossify in *nkx3.2*$^{-/-}$ without apparent delay.

131 The lower jaws are increasingly turned downward in *nkx3.2*$^{-/-}$ by the end of the first month,
132 resulting in a greater gape (Fig. 2d, e). The jaw joint is still absent in *nkx3.2*$^{-/-}$ mutants: a sheet of
133 perichondrium lies between the ossifying quadrate and articular — so the two bones remain distinct
134 elements — but this interface has none of those essential components of synovial diarthrosis (Fig. 2n).
135 Many other osteological differences emerge by this stage. Normally, the premaxilla and the maxilla
136 swing forward to sit nearly vertical and are hinged by the kinethmoid for suction feeding (Hernandez,
137 2000; Hernandez et al., 2007) (Fig. 2c). In *nkx3.2*$^{-/-}$ mutants, however, the premaxilla and the maxilla
138 are oriented posteroventrally and abutted against the anterior margin of the orbit (Fig. 2d). The
139 kinethmoid is reduced into a fused bony process, unlike a rod-like hinge element in wildtype
140 (Hernandez et al., 2007). The downturned lower jaws of the *nkx3.2*$^{-/-}$ mutants are relatively shorter than
141 the normal lower jaws of wildtypes. The basihyal protrudes anteroventrally as much as the lower jaw,
142 implying that the muscle connecting those two elements (m. intermandibularis posterior) (Schilling and
143 Kimmel, 1997) may be responsible for the lower jaw orientation. As a result of these modifications,
144 *nkx3.2*$^{-/-}$ mutants have a shorter snout, a fixed open gape, and a dorsoventrally tall profile.
145 Morphological variations within a cohort of *nkx3.2*$^{-/-}$ mutants is greatest at this stage than in any other,
146 as indicated by the range of variation in lower jaw depression (Fig. 2o).
147

148 **The adult *nkx3.2*$^{-/-}$ phenotype accommodates functional jaw loss**

149 At 2 months of age and approaching sexual maturity nearly all *nkx3.2*$^{-/-}$ mutants have a gape angle
150 greater than 90 degrees (Fig. 2o). These *nkx3.2*$^{-/-}$ adults continue to be characterized by the
151 morphological differences identified at 1 mpf. The nostrils sit between the eyes as the snout is reduced

152 in length relative to wildtype zebrafish. The skulls appear to be more highly ossified in *nkx3.2*$^{-/-}$
153 mutants than in wildtype, where massive bones and cartilages are identified around the interface of
154 quadrate and articular, in the lower branchial region, and in the laterally expanded operculum (Figs. 2j,
155 g, 3b; Movie 1). All homozygous mutants showed the descriptive skeletal traits identified here.
156 Morphologically, the two alleles (*nkx3.2*^{ua5011} and *nkx3.2*^{el802}) are virtually indistinguishable from each
157 other at respective ages (Figs. 2j, k, g, 3b), given variations within a strain (for examples, see variation
158 in gape angles or sexual dimorphism in *nkx3.2*^{ua5011}: Figs. 2o, 3g).

159 With the modified skulls, adult *nkx3.2*$^{-/-}$ mutants exhibit feeding behaviors markedly different
160 from wildtype (Movie 1). Wildtype zebrafish feed by suction using rapid lower jaw depression and
161 forward swing of the mobile premaxilla-maxilla complex, consistent with general teleost feeding
162 mechanics. In contrast, adult *nkx3.2*$^{-/-}$ mutants are constrained by the fixed upper jaw unit and open
163 gape. They instead show ram feeding behaviors (swimming through food).

164 This behavior is correlated with the skull remodeling in *nkx3.2*$^{-/-}$ mutants. In zebrafish skulls,
165 the bones form endochondrally (quadrate, anguloarticular, basihyal) or intramembranously (premaxilla,
166 maxilla, dentary, jugal, opercular, preopercular) (Cubbage and Mabee, 1996; Schilling and Kimmel,
167 1997). Much of the skeletal remodeling observed in adult *nkx3.2*$^{-/-}$ mutants occurs in the
168 intramembranous bones — spatially and temporarily well outside the known expression domain of
169 *nkx3.2* (Askary et al., 2017; Miller et al., 2003). Until past 1 mpf, the fusion between jaw cartilages is
170 not completely ossified in these mutants, potentially allowing plastic remodeling (Fig. 2e, l). These
171 observations support that *nkx3.2*$^{-/-}$ zebrafish accommodate functional jawlessness through remodeling
172 of the skull and changes to feeding behavior.

173

174 ***nkx3.2*$^{-/-}$ zebrafish converge onto some ancient agnathans in overall head shapes**

175 Through this dramatic remodeling of the skull, *nkx3.2*$^{-/-}$ zebrafish assume a head shape reminiscent of
176 two lineages of extinct jawless vertebrates that have laterally compressed body profiles: birkeniiform

177 anaspids (Fig. 3c), stem cyclostomes known mostly from the Silurian period (Blom et al., 2001;
178 Miyashita et al., 2019); and furcacaudiid thelodonts (Fig. 3d), much more elusive stem gnathostomes
179 known from the Silurian and Devonian periods (excluded from quantitative comparison; see Methods
180 for rationales) (Märss et al., 2007; Wilson and Caldwell, 1998). Qualitatively, the resemblance is
181 particularly striking in overall head shape characters, including: fixed gape (depressed lower lips),
182 shortened snout, interorbital position of nostril, proportionally large branchial region, and massive
183 parietal region behind the occiput.

184 In linear morphometrics, the gape angle between upper and lower lips reveals that *nkx3.2*$^{-/-}$
185 mutants assimilates the anaspid-like condition late in ontogeny (Fig. 2o). The trait in *nkx3.2*$^{-/-}$ mutants
186 departs from that in wildtype after the onset of skull ossification and active feeding, and overlaps with
187 the range occupied by anaspids (grey zone in Fig. 2o). When the jaws are at rest, the gape angle in
188 wildtype zebrafish is consistently around 30 degrees regardless of ontogenetic stages. This is also the
189 case for the *nkx3.2*$^{-/-}$ mutants at 4 and 14 dpf when they still rely on yolk as main intake. The gape
190 angle increases steadily thereafter.

191 In landmark-based geometric morphometrics, *nkx3.2*$^{-/-}$ mutants aligned more closely with
192 anaspids than wildtype along the principal components (PCs) that explain the adult phenotype (PCs 1
193 and 5) (Fig. 3e). Nearly one third of the overall shape variation loads on PC1 and primarily concerns
194 anteroposterior length and dorsoventral height of the entire head. Compared to wildtype zebrafish,
195 *nkx3.2*$^{-/-}$ mutants and most anaspids have a much shorter snout (with the lips and the nostrils shifting
196 posteriorly toward the eye) and dorsoventrally deeper lower lips. PC 5 explains 7.0 % of the overall
197 shape variation, and the traits that vary along it are orientation of lower lip and relative height of
198 nostrils, which clearly set wildtype zebrafish apart from *nkx3.2*$^{-/-}$ mutants and anaspids. On the
199 Cartesian grid of PCs 1 and 5, *nkx3.2*$^{-/-}$ mutants overlap with anaspids in morphospace occupation and
200 apart from wildtype zebrafish (Fig. 3f). The area of overlap also indicates that *nkx3.2*$^{-/-}$ mutants are
201 broadly similar to anaspids in these PCs, not just to one or a few individual anaspid taxa. PCs 2-4 (not

202 shown in Fig. 3) largely explain variations among anaspids or within wildtype/mutant zebrafish
203 samples and therefore uninformative for comparison between the groups (datasets containing landmark
204 coordinates and Procrustes transformation are provided in Data Supplement 2).
205
206 **Discussion**
207
208 **Mutants corroborate the function of *nkx3.2* in joint development**
209 Our *nkx3.2*$^{-/-}$ zebrafish reinforce the morphant-based insight that this transcription factor is essential to
210 the development of jaw joint in non-mammalian jawed vertebrates (Miller et al., 2003). This is likely
211 the widespread condition among jawed vertebrates. *Nkx3.2* knockdown also results in fusion between
212 the palatoquadrate and Meckel's cartilage in amphibians (Lukas and Olsson, 2018a), and similar
213 phenotype is observed in chicks with ectopic expression of BMP4 and FGF8 that repressed *Nkx3.2*
214 (Wilson and Tucker, 2004). In mammals, the palatoquadrate (malleus) and Meckel's cartilage (incus)
215 migrate to form middle ear ossicles. The malleus-incus joint is not affected in *Nkx3.2*$^{-/-}$ mice, although
216 the malleus becomes narrower in the mutants, and although *Nkx3.2* plays a role in specification of the
217 gonium and the anterior tympanic ring (Tucker et al., 2004). Aside from the head, *Nkx3.2* plays a role
218 in various structures in mice and chicks, including axial column (Herbrand et al., 2002; Lettice et al.,
219 2001; Murtaugh et al., 2001) and visceral lateralities of spleen and pancreas (Hecksher-Sørensen et al.,
220 2004; Schneider et al., 1999). We will test whether or not *nkx3.2*$^{-/-}$ zebrafish have parallel phenotypes
221 to these amniote mutants in a forthcoming work.
222 During development of the jaw joint, *nkx3.2* has been posited to specify the joint interzone by
223 inhibiting maturation or hypertrophy of the chondrocytes (Miller et al., 2003; Smeeton et al., 2016).
224 Similar function has been described for *irx7* and *irx5a* in the hyoid joint (Askary et al., 2015). This is
225 consistent with the predicted regulatory function of *Nkx3.2* in vertebral development, intervertebral and
226 interphalangeal joint formation, or somatic chondrogenesis in general (Herbrand et al., 2002; Lettice et

227 al., 2001; Murtaugh et al., 2001) — via repression of *Runx2*, by upregulating *Col2α1*, and/or through a
228 positive feedback loop with *Sox9* (Smeeton et al., 2016). These insights are based on: a) experimental
229 results using amniote embryos or somitic mesodermal cell cultures (Cairns et al., 2008; Kawato et al.,
230 2012; Lengner et al., 2005; Murtaugh et al., 2001; Provot et al., 2006; Yamashita et al., 2009; Zeng et
231 al., 2002); and b) clinical and genetic studies of human pathologies, including osteoarthritis and
232 spondylo-megaepiphyseal-metaphyseal dysplasia (including pseudoepiphyses) (Caron et al., 2015;
233 Hellemans et al., 2009). Before this study, however, no mutants were available to specifically address
234 these potential mechanisms of *nkx3.2* functions in the mandibular arch.
235

236 **The open-mouth phenotype results from plastic remodeling**

237 The late onset and topology of skull/jaw remodeling suggests that *nkx3.2*$^{-/-}$ zebrafish accommodate the
238 loss of the jaw joint in a plastic response. Other than the absence of jaw joint, *nkx3.2*$^{-/-}$ zebrafish appear
239 otherwise normal until metamorphosis (14–21 dpf) (Fig. 1d, g). As the skull ossifies, however, the
240 observed phenotype becomes increasingly prominent (Fig. 2b, d, g, j). Although the fused jaw
241 cartilages clearly result from *nkx3.2* mutation, it seems unlikely that *nkx3.2* loss-of-function, by itself,
242 yields all the rest of phenotypic effects described here. A genome-wide analysis suggests that *nkx3.2*
243 patterning effects in the skull are restricted to the mid-portion of the mandibular arch (Askary et al.,
244 2017). Nor does *nkx3.2* have known expression or function in the intramembranously ossified skull
245 elements (Miller et al., 2003; Tucker et al., 2004), which are dramatically modified in our *nkx3.2*$^{-/-}$ fish.
246 The hypertrophied mandibular cartilage may result from *nkx3.2* loss-of-function in regulating local
247 chondrogenesis (Smeeton et al., 2016). Still, further investigation is warranted because in amphibians
248 an ectopic cartilage formed in the mandibular arch with *Nkx3.2* overexpression, not repression (Lukas
249 and Olsson, 2018b).

250 Comparative survey across vertebrates supports our interpretation of the adult *nkx3.2*$^{-/-}$
251 phenotype as skeletal remodeling to accommodate the jaw joint loss. Discrete variation in cichlid jaw

252 morphology has an epigenetic basis in behaviorally mediated skeletal remodeling, where gaping
253 frequencies in juveniles correlate with dimensions of the retroarticular process (Hu and Albertson,
254 2017). The magnitude of morphological changes in the adult *nkx3.2*$^{-/-}$ phenotype also appears
255 consistent with a series of surgical experiments in mammalian jaw skeletons (Bayram et al., 2010;
256 Gomes et al., 2012; Horowitz and Shapiro, 1955; Lifshitz, 1976; Miyazaki et al., 2016; Rodrigues et
257 al., 2009; Sarnat, 1970; Sarnat and Muchnic, 1971; Toledo et al., 2014) or with the 'bird face'
258 deformity observed in clinical cases of the temporomandibular joint ankylosis in humans (El-Sheikh et
259 al., 1996). Collectively, these studies show that latent potentials of development allow a plastic trait to
260 become expressed. Variations resulting from developmental plasticities — whether induced by
261 environmental cue, developmental perturbation, or mutation — are often non-random and adaptive
262 (West-Eberhard, 2005a, 2005b, 2003), as documented across wide ranges of taxa and structures
263 including cichlid jaw skeletons (Hu and Albertson, 2017; Stewart and Albertson, 2010). Ram feeding
264 facilitated by the fixed open gape in the adult *nkx3.2*$^{-/-}$ zebrafish corroborates non-random, adaptive
265 accommodation of the jaw joint defect.
266

267 **Jaw joint functions constrain skull morphology in vertebrates**

268 The drastically remodeled skull of adult *nkx3.2*$^{-/-}$ zebrafish highlights jaw joint functions as an
269 important factor in morphological diversity of jawed vertebrate skulls (Depew et al., 2005; Depew and
270 Compagnucci, 2008; Depew and Simpson, 2006). Simultaneously, the absence of jaw joint (or jaw
271 apparatus altogether) also limits functionally viable forms. This is implied by the superficial
272 convergence in head shapes between *nkx3.2*$^{-/-}$ zebrafish and two Paleozoic agnathan lineages (anaspids
273 and furcacaudiform thelodonts). The *nkx3.2*$^{-/-}$ zebrafish and these agnathans share a functional
274 requirement — the absence of a hinge joint between upper and lower lips — and transversely
275 compressed body profile. No evidence suggests any more similarities in the otherwise wildtype-like
276 young mutants (Fig. 1d, g) until the lower jaw skeletons begin rotating posteroventrally post 14 dpf

277 (Fig. 2b, d). Therefore, we interpret the anaspid/thelodont-like traits in the adult *nkx3.2*$^{-/-}$ zebrafish not
278 as recapitulations of conserved early vertebrate development (atavism), but instead as assimilations of
279 the patterns previously exploited by early vertebrates in a zebrafish skull (convergence).

280 Thus, the jaw joint loss (*nkx3.2* loss-of-function phenotype) released *nkx3.2*$^{-/-}$ zebrafish from
281 forms that can facilitate jaw movement, and exposed them to a different functional requirement of
282 feeding without mobile jaws. A fixed open gape — accompanied by modification of the skull elements
283 — is one morphological solution to the functional loss of jaw joint, which is corroborated by ram
284 feeding exhibited by *nkx3.2*$^{-/-}$ mutants (Movie 1). The magnitude of modification documented post-
285 hatching (Figs. 1, 2) is a testament to significant functional optimization within the bounds of the
286 gnathostome bauplan. Simultaneously, well-constrained occupancy by the *nkx3.2*$^{-/-}$ in the PCA plot
287 (Fig. 3f) implies that alternative morphological patterns are either functionally non-viable (e.g., fixed
288 closed gape) or developmentally non-accesible (e.g., ectopic formation of a mouth). Thus, the *nkx3.2*$^{-/-}$
289 mutants provide a rare case study. The results suggest that the vertebrate bauplan allows a limited
290 repertoire of functionally viable morphological patterns, onto which forms may converge under a given
291 functional constraint.

292 In support of our interpretation, remarkable convergences arise via developmental plasticity
293 under similar functional requirements — even in the absence of homology in individual skeletal
294 elements — between taxa widely separated chronologically and phylogenetically. Bichirs (*Polypterus*)
295 routinely trained under terrestrial conditions modify the pectoral fin skeleton through plasticity and
296 develop morphological conditions observed in stem tetrapods (Standen et al., 2014). In another, *vav2*
297 and *waslb* mutant zebrafish develop limb-like long bones connected by joints within the pectoral fins
298 (Hawkins et al., 2018). As shown in *nkx3.2*$^{-/-}$ zebrafish, these experimental manipulations illustrate
299 through phenotypic accommodation that functions are a strong constraint for adaptive forms, even after
300 development has laid out phylogenetically conserved patterns (such as homologies of the individual
301 bones).

302

303 ***nkx3.2* mutants as a unique model for skeletal development and disease**

304 Mechanisms of developmentally plastic remodeling, whether at the level of whole-animal behavior or
305 gene transcription, remain an elusive component of skeletal development that is challenging to test
306 experimentally. Therefore, *nkx3.2*$^{-/-}$ zebrafish provide a unique experimental system in which to test the
307 role of a joint in skeletal development further. For example, further investigations are warranted to
308 determine precisely: a) what genetic mechanisms regulate the remodeling of intramembranous
309 ossifications; b) what components of the remodeling process respond to the jaw joint dysfunction; and
310 c) whether any feedback exists to coordinate remodeling between developmentally independent, but
311 functionally connected units (e.g., premaxilla-maxilla complex and kinethmoid). Such insights would
312 begin to fill in knowledge gaps regarding skeletal and joint diseases including osteoarthritis and joint
313 ankylosis.

314 The non-atavistic nature of the *nkx3.2*$^{-/-}$ phenotype is potentially useful to reevaluate
315 evolutionarily inspired interpretations of phenocopies in general. There are no evolutionary
316 relationships in the similarities between *nkx3.2*$^{-/-}$ zebrafish and anaspids or thelodonts. Anaspids are a
317 stem cyclostome lineage (Miyashita et al., 2019) (Fig. 3g), and thus a poor surrogate for an ancestral
318 state. The lineages between anaspids and thelodonts, or those between thelodonts and the gnathostome
319 crown, do not share a similar combination of morphological traits, but instead are dorsoventrally
320 depressed forms (Janvier, 1996; Miyashita, 2016; Miyashita et al., 2019) (Fig. 3g). Finally, head
321 similarities between the mutants and the stem taxa do not extend beyond overall configuration. No
322 skull elements are lost or replaced in *nkx3.2*$^{-/-}$ zebrafish to achieve the anaspid/thelodont-like
323 micromery (Blom et al., 2001; Janvier, 1996; Märss et al., 2007). Therefore, in no way does the adult
324 *nkx3.2*$^{-/-}$ phenotype represent a reversal to an ancestral state. Although experimental phenocopies are
325 often interpreted as atavistic (ancestral reversal), alternative interpretations are seldom tested (Smith
326 and Schneider, 1998). Here, our *nkx3.2*$^{-/-}$ zebrafish present developmental plasticity as a testable

alternative to atavistic reversal to explain a phenocopy. By showing that a gnathostome can survive without a jaw, the anaspid/thelodont-like *nkx3.2*$^{-/-}$ zebrafish also offer a comparative model to make inferences about the functional morphology of these long-extinct agnathans.

Data availability. Sequence information, measurements, and landmark coordinates are available as data supplements to this paper.

Author contributions. T.M. conceived project; T.M. and A.P.O. performed experiments resulting in *nkx3.2*^{ua5011}; J.S. and N.N. performed experiments resulting in *nkx3.2*^{el802}; P.B. and B.G. provided µCT scanning and histological sampling; T.M. and P.B. conducted morphometric analyses; T.M., P.B., A.R.P., J.G.C., D.G., and W.T.A. analyzed data; T.M. wrote the paper with inputs from P.B., A.P.O., J.S., A.R.P., J.G.C., D.G., and W.T.A.

Competing interests. We have no competing interests.

Funding. This work was supported by Natural Science and Engineering Research Council grants RGPIN-2014-04863, RGPIN-2014-06311, and RGPIN-2015-06006 (to A.R.P., D.G., and W.T.A., respectively) and National Institute of Health grants R35DE027550 and K99 DE027218 (to J.G.C. and J.S., respectively).

Acknowledgements. We thank B.F. Eames (University of Saskatchewan) for facilitating our collaboration.

352 **References**

353 Adekeye EO. 1983. Ankylosis of the mandible: Analysis of 76 cases. *Journal of Oral and*
354 *Maxillofacial Surgery* **41**:442–449. doi:10.1016/0278-2391(83)90129-5

355 Askary A, Mork L, Paul S, He X, Izuhara AK, Gopalakrishnan S, Ichida JK, McMahon AP,
356 Dabizljevic S, Dale R, Mariani FV, Crump JG. 2015. Iroquois proteins promote skeletal joint
357 formation by maintaining chondrocytes in an immature state. *Developmental Cell* **35**:358–365.
358 doi:10.1016/j.devcel.2015.10.004

359 Askary A, Xu P, Barske L, Bay M, Bump P, Balczerski B, Bonaguidi MA, Crump JG. 2017. Genome-
360 wide analysis of facial skeletal regionalization in zebrafish. *Development* **144**:2994–3005.
361 doi:10.1242/dev.151712

362 Barske L, Askary A, Zuniga E, Balczerski B, Bump P, Nichols JT, Crump JG. 2016. Competition
363 between Jagged-Notch and Endothelin1 signaling selectively restricts cartilage formation in the
364 zebrafish upper face. *PLoS Genet* **12**:e1005967. doi:10.1371/journal.pgen.1005967

365 Bayram B, Uckan S, Cetinsahin A, Arman Ozcirpici A, Ozdemir H, Yazici C. 2010. Repositioning of
366 the masseter muscle and its effect on skeletal growth. *Oral Surgery, Oral Medicine, Oral*
367 *Pathology, Oral Radiology, and Endodontology* **109**:e1–e5. doi:10.1016/j.tripleo.2009.12.041

368 Bixler D, Ward R, Gale DD. 1985. Agnathia-holoprosencephaly: a developmental field complex
369 involving face and brain. Report of 3 cases. *J Craniofac Genet Dev Biol Suppl* **1**:241–249.

370 Blom H, Märss T. 2010. The interrelationships and evolutionary history of anaspid fishes In: Elliott
371 DK, Maisey JG, Yu X, Miao D, editors. Morphology, Phylogeny and Palaeogeography of
372 Fossil Fishes – Honoring Meemann Chang. Munich: Verlag Dr. Fredrich Pfeil.

373 Blom H, Märss T, Miller CG. 2001. Silurian and earliest Devonian birkeniid anaspids from the
374 Northern Hemisphere. *Earth and Environmental Science Transactions of The Royal Society of*
375 *Edinburgh* **92**:263–323. doi:10.1017/S0263593300000250

376 Brown DM, Marsh JL. 1990. Agnathia and Associated Malformations: A Case Report. *Cleft Palate*
377 *Journal* **27**:415–418. doi:10.1597/1545-1569_1990_027_0415_aaamac_2.3.co_2

378 Cairns DM, Sato ME, Lee PG, Lassar AB, Zeng L. 2008. A gradient of Shh establishes mutually
379 repressing somitic cell fates induced by Nkx3.2 and Pax3. *Developmental Biology* **323**:152–
380 165. doi:10.1016/j.ydbio.2008.08.024

381 Caron MMJ, Emans PJ, Surtel DAM, van der Kraan PM, van Rhijn LW, Welting TJM. 2015. BAPX-
382 1/NKX-3.2 acts as a chondrocyte hypertrophy molecular switch in osteoarthritis. *Arthritis &*
383 *Rheumatology* **67**:2944–2956. doi:10.1002/art.39293

384 Cerny R, Cattell M, Sauka-Spengler T, Bronner-Fraser M, Yu F, Medeiros DM. 2010. Evidence for the
385 prepattern/cooption model of vertebrate jaw evolution. *PNAS* **107**:17262–17267.
386 doi:10.1073/pnas.1009304107

387 Chidzonga MM. 1999. Temporomandibular joint ankylosis: review of thirty-two cases. *British Journal*
388 *of Oral and Maxillofacial Surgery* **37**:123–126. doi:10.1054/bjom.1997.0089

389 Cubbage CC, Mabee PM. 1996. Development of the cranium and paired fins in the zebrafish *Danio*
390 *rerio* (Ostariophysi, Cyprinidae). *Journal of Morphology* **229**:121–160.
391 doi:10.1002/(SICI)1097-4687(199608)229:2<121::AID-JMOR1>3.0.CO;2-4

392 Depew MJ, Compagnucci C. 2008. Tweaking the hinge and caps: testing a model of the organization of
393 jaws. *J Exp Zool* **310B**:315–335. doi:10.1002/jez.b.21205

394 Depew MJ, Simpson CA. 2006. 21st Century neontology and the comparative development of the
395 vertebrate skull. *Dev Dyn* **235**:1256–1291. doi:10.1002/dvdy.20796

396 Depew MJ, Simpson CA, Morasso M, Rubenstein JLR. 2005. Reassessing the Dlx code: the genetic
397 regulation of branchial arch skeletal pattern and development. *Journal of Anatomy* **207**:501–
398 561. doi:10.1111/j.1469-7580.2005.00487.x

399 Donoghue PCJ, Forey PL, Aldridge RJ. 2000. Conodont affinity and chordate phylogeny. *Biological*
400 *Reviews* **75**:191–251. doi:null

401 El-Sheikh MM, Medra AM, Warda MH. 1996. Bird face deformity secondary to bilateral
402 temporomandibular joint ankylosis. *Journal of Cranio-Maxillofacial Surgery* **24**:96–103.
403 doi:10.1016/S1010-5182(96)80020-5

404 Gagnon JA, Valen E, Thyme SB, Huang P, Ahkmetova L, Pauli A, Montague TG, Zimmerman S,
405 Richter C, Schier AF. 2014. Efficient mutagenesis by Cas9 protein-mediated oligonucleotide
406 insertion and large-scale assessment of single-guide RNAs. *PLOS ONE* **9**:e98186.
407 doi:10.1371/journal.pone.0098186

408 Gekas J, Li B, Kamnasaran D. 2010. Current perspectives on the etiology of agnathia-otocephaly.
409 *European Journal of Medical Genetics* **53**:358–366. doi:10.1016/j.ejmg.2010.09.002

410 Gillis JA, Modrell MS, Baker CVH. 2013. Developmental evidence for serial homology of the
411 vertebrate jaw and gill arch skeleton. *Nat Commun* **4**:1436. doi:10.1038/ncomms2429

412 Gomes FEF, Moraes RB, Luz JG de C. 2012. Effects of temporal muscle detachment and
413 coronoidotomy on facial growth in young rats. *Brazilian Oral Research* **26**:348–354.
414 doi:10.1590/S1806-83242012000400011

415 Hall BK. 2015. Bones and Cartilage: Developmental and Evolutionary Skeletal Biology. 2nd edition.
416 London: Academic Press.

417 Hawkins MB, Henke K, Harris MP. 2018. Latent developmental potential to form limb-like skeletal
418 structures in zebrafish. *bioRxiv* 450619. doi:10.1101/450619

419 Hecksher-Sørensen J, Watson RP, Lettice LA, Serup P, Eley L, Angelis CD, Ahlgren U, Hill RE. 2004.
420 The splanchnic mesodermal plate directs spleen and pancreatic laterality, and is regulated by
421 Bapx1/Nkx3.2. *Development* **131**:4665–4675. doi:10.1242/dev.01364

422 Hellemans J, Simon M, Dheedene A, Alanay Y, Mihci E, Rifai L, Sefiani A, van Bever Y, Meradji M,
423 Superti-Furga A, Mortier G. 2009. Homozygous inactivating mutations in the NKX3-2 gene
424 result in spondylo-megaepiphyseal-metaphyseal dysplasia. *The American Journal of Human*
425 *Genetics* **85**:916–922. doi:10.1016/j.ajhg.2009.11.005

426 Herbrand H, Pabst O, Hill R, Arnold H-H. 2002. Transcription factors Nkx3.1 and Nkx3.2 (Bapx1)
427 play an overlapping role in sclerotomal development of the mouse. *Mechanisms of*
428 *Development* **117**:217–224. doi:10.1016/S0925-4773(02)00207-1

429 Hernandez LP. 2000. Intraspecific scaling of feeding mechanics in an ontogenetic series of zebrafish,
430 *Danio rerio*. *Journal of Experimental Biology* **203**:3033–3043.

431 Hernandez LP, Bird NC, Staab KL. 2007. Using zebrafish to investigate cypriniform evolutionary
432 novelties: Functional development and evolutionary diversification of the kinethmoid. *Journal*
433 *of Experimental Zoology Part B: Molecular and Developmental Evolution* **308B**:625–641.
434 doi:10.1002/jez.b.21166

435 Horowitz SL, Shapiro HH. 1955. Modification of skull and jaw architecture following removal of the
436 masseter muscle in the rat. *American Journal of Physical Anthropology* **13**:301–308.
437 doi:10.1002/ajpa.1330130208

438 Howland HC, Merola S, Basarab JR. 2004. The allometry and scaling of the size of vertebrate eyes.
439 *Vision Research* **44**:2043–2065. doi:10.1016/j.visres.2004.03.023

440 Hu Y, Albertson RC. 2017. Baby fish working out: an epigenetic source of adaptive variation in the
441 cichlid jaw. *Proc R Soc B* **284**:20171018. doi:10.1098/rspb.2017.1018

442 Janvier P. 2007. Homologies and evolutionary transitions in early vertebrate history In: Anderson JS,
443 Sues H-D, editors. Major Transitions in Vertebrate Evolution. Bloomington: Indiana University
444 Press. pp. 57–121.

445 Janvier P. 1996. Early Vertebrates, Oxford Monographs on Geology and Geophysics. Oxford:
446 Clarendon Press.

447 Kawato Y, Hirao M, Ebina K, Shi K, Hashimoto J, Honjo Y, Yoshikawa H, Myoui A. 2012. Nkx3.2
448 promotes primary chondrogenic differentiation by upregulating Col2a1 transcription. *PLOS*
449 *ONE* **7**:e34703. doi:10.1371/journal.pone.0034703

450 Keating JN, Donoghue PCJ. 2016. Histology and affinity of anaspids, and the early evolution of the
451 vertebrate dermal skeleton. *Proc R Soc B* **283**:20152917. doi:10.1098/rspb.2015.2917

452 Kimmel CB, Ballard WW, Kimmel SR, Ullmann B, Schilling TF. 1995. Stages of embryonic
453 development of the zebrafish. *Dev Dyn* **203**:253–310. doi:10.1002/aja.1002030302

454 Klingenberg CP. 2011. MorphoJ: an integrated software package for geometric morphometrics.
455 *Molecular Ecology Resources* **11**:353–357. doi:10.1111/j.1755-0998.2010.02924.x

456 Kuratani S. 2012. Evolution of the vertebrate jaw from developmental perspectives. *Evolution &*
457 *Development* **14**:76–92. doi:10.1111/j.1525-142X.2011.00523.x

458 Labun K, Montague TG, Gagnon JA, Thyme SB, Valen E. 2016. CHOPCHOP v2: a web tool for the
459 next generation of CRISPR genome engineering. *Nucleic Acids Res* **44**:W272–W276.
460 doi:10.1093/nar/gkw398

Lengner CJ, Hassan MQ, Serra RW, Lepper C, Wijnen AJ van, Stein JL, Lian JB, Stein GS. 2005. Nkx3.2-mediated repression of Runx2 promotes chondrogenic differentiation. *J Biol Chem* **280**:15872–15879. doi:10.1074/jbc.M411144200

Lettice L, Hecksher-Sørensen J, Hill R. 2001. The role of Bapx1 (Nkx3.2) in the development and evolution of the axial skeleton. *Journal of Anatomy* **199**:181–187. doi:10.1046/j.1469-7580.2001.19910181.x

Lifshitz J. 1976. Comparative anatomic study of mandibular growth in rats after bilateral resections of superficial masseter, posterior temporal, and anterior digastric muscles. *J Dent Res* **55**:854–858. doi:10.1177/00220345760550052301

Lukas P, Olsson L. 2018a. Bapx1 is required for jaw joint development in amphibians. *Evolution & Development* **20**:192–206. doi:10.1111/ede.12267

Lukas P, Olsson L. 2018b. Bapx1 upregulation is associated with ectopic mandibular cartilage development in amphibians. *Zoological Letters* **4**:16. doi:10.1186/s40851-018-0101-3

Manganello-Souza LC, Mariani PB. 2003. Temporomandibular joint ankylosis: Report of 14 cases. *International Journal of Oral and Maxillofacial Surgery* **32**:24–29. doi:10.1054/ijom.2002.0308

Märss T, Turner S, Karatajūtė-Talimaa V. 2007. Handbook of Paleoichthyology / "Agnatha" II. Thelodonti. München: Verlag Dr. Friedrich Pfeil.

Medeiros DM, Crump JG. 2012. New perspectives on pharyngeal dorsoventral patterning in development and evolution of the vertebrate jaw. *Developmental Biology* **371**:121–135. doi:10.1016/j.ydbio.2012.08.026

Miller CT, Yelon D, Stainier DYR, Kimmel CB. 2003. Two endothelin 1 effectors, hand2 and bapx1, pattern ventral pharyngeal cartilage and the jaw joint. *Development* **130**:1353–1365. doi:10.1242/dev.00339

Miyashita T. 2016. Fishing for jaws in early vertebrate evolution: A novel hypothesis of mandibular confinement. *Biological Reviews* **91**:611–657. doi:10.1111/brv.12187

Miyashita T. 2012. Comparative Analysis of the Anatomy of the Myxinoidea and the Ancestry of Early Vertebrate Lineages (Unpublished M.Sc. thesis). Edmonton: University of Alberta.

Miyashita T, Coates MI, Farrar R, Larson P, Manning PL, Wogelius RA, Edwards NP, Anné J, Bergmann U, Palmer AR, Currie PJ. 2019. Hagfish from the Cretaceous Tethys Sea and a reconciliation of the morphological–molecular conflict in early vertebrate phylogeny. *PNAS* **116**:2146–2151. doi:10.1073/pnas.1814794116

Miyazaki M, Yonemitsu I, Takei M, Kure-Hattori I, Ono T. 2016. The imbalance of masticatory muscle activity affects the asymmetric growth of condylar cartilage and subchondral bone in rats. *Archives of Oral Biology* **63**:22–31. doi:10.1016/j.archoralbio.2015.11.020

496 Montague TG, Cruz JM, Gagnon JA, Church GM, Valen E. 2014. CHOPCHOP: a CRISPR/Cas9 and
497 TALEN web tool for genome editing. *Nucleic Acids Res* **42**:W401–W407.
498 doi:10.1093/nar/gku410

499 Murtaugh LC, Zeng L, Chyung JH, Lassar AB. 2001. The chick transcriptional repressor Nkx3.2 acts
500 downstream of Shh to promote BMP-dependent axial chondrogenesis. *Developmental Cell*
501 **1**:411–422. doi:10.1016/S1534-5807(01)00039-9

502 Provot S, Kempf H, Murtaugh LC, Chung U, Kim D-W, Chyung J, Kronenberg HM, Lassar AB. 2006.
503 Nkx3.2/Bapx1 acts as a negative regulator of chondrocyte maturation. *Development* **133**:651–
504 662. doi:10.1242/dev.02258

505 Rodrigues L, Traina AA, Nakamai LF, Luz JG de C. 2009. Effects of the unilateral removal and
506 dissection of the masseter muscle on the facial growth of young rats. *Brazilian Oral Research*
507 **23**:89–95. doi:10.1590/S1806-83242009000100015

508 Rohlf FJ. 2018. tpsDIG. New York.

509 Rohlf FJ. 1999. Shape Statistics: Procrustes Superimpositions and Tangent Spaces. *J of Classification*
510 **16**:197–223. doi:10.1007/s003579900054

511 Sansom RS, Freedman K, Gabbott SE, Aldridge RJ, Purnell MA. 2010. Taphonomy and affinity of an
512 enigmatic Silurian vertebrate, *Jamoytius kerwoodi* White. *Palaeontology* **53**:1393–1409.
513 doi:10.1111/j.1475-4983.2010.01019.x

514 Sarnat BG. 1970. The face and jaws after surgical experimentation with the septovomeral region in
515 growing and adult rabbits. *Acta Oto-Laryngologica* **69**:1–30. doi:10.3109/00016487009131762

516 Sarnat BG, Muchnic H. 1971. Facial skeletal changes after mandibular condylectomy in the adult
517 monkey. *J Anat* **108**:323–338.

518 Schiffer C, Tariverdian G, Schiesser M, Thomas MC, Sergi C. 2002. Agnathia-otocephaly complex:
519 Report of three cases with involvement of two different Carnegie stages. *American Journal of*
520 *Medical Genetics* **112**:203–208. doi:10.1002/ajmg.10672

521 Schilling TF, Kimmel CB. 1997. Musculoskeletal patterning in the pharyngeal segments of the
522 zebrafish embryo. *Development* **124**:2945–2960.

523 Schneider A, Mijalski T, Schlange T, Dai W, Overbeek P, Arnold H-H, Brand T. 1999. The homeobox
524 gene it NKX3.2 is a target of left–right signalling and is expressed on opposite sides in chick
525 and mouse embryos. *Current Biology* **9**:911-S1. doi:10.1016/S0960-9822(99)80397-2

526 Smeeton J, Askary A, Gage Crump J. 2016. Building and maintaining joints by exquisite local control
527 of cell fate. *WIREs Dev Biol* **6**:e245. doi:10.1002/wdev.245

528 Smith KK, Schneider RA. 1998. Have gene knockouts caused evolutionary reversals in the mammalian
529 first arch? *BioEssays* **20**:245–255. doi:10.1002/(SICI)1521-1878(199803)20:3<245::AID-
530 BIES8>3.0.CO;2-Q

531 Standen EM, Du TY, Larsson HCE. 2014. Developmental plasticity and the origin of tetrapods. *Nature*
532 **513**:54–58. doi:10.1038/nature13708

533 Stewart TA, Albertson RC. 2010. Evolution of a unique predatory feeding apparatus: Functional
534 anatomy, development and a genetic locus for jaw laterality in Lake Tanganyika scale-eating
535 cichlids. *BMC Biology* **8**:8. doi:10.1186/1741-7007-8-8

536 Toledo LG, Cavalcanti SCXB, Corrêa L, Luz JGC. 2014. Effects of injury or removal of the articular
537 disc on maxillomandibular growth in young rats. *Journal of Oral and Maxillofacial Surgery*
538 **72**:2140–2147. doi:10.1016/j.joms.2014.06.445

539 Tucker AS, Watson RP, Lettice LA, Yamada G, Hill RE. 2004. Bapx1 regulates patterning in the
540 middle ear: Altered regulatory role in the transition from the proximal jaw during vertebrate
541 evolution. *Development* **131**:1235–1245. doi:10.1242/dev.01017

542 West-Eberhard MJ. 2005a. Developmental plasticity and the origin of species differences. *PNAS*
543 **102**:6543–6549. doi:10.1073/pnas.0501844102

544 West-Eberhard MJ. 2005b. Phenotypic accommodation: adaptive innovation due to developmental
545 plasticity. *Journal of Experimental Zoology Part B: Molecular and Developmental Evolution*
546 **304B**:610–618. doi:10.1002/jez.b.21071

547 West-Eberhard MJ. 2003. Developmental Plasticity and Evolution, 1 edition. ed. Oxford ; New York:
548 Oxford University Press.

549 Wilson J, Tucker AS. 2004. Fgf and Bmp signals repress the expression of Bapx1 in the mandibular
550 mesenchyme and control the position of the developing jaw joint. *Developmental Biology*
551 **266**:138–150. doi:10.1016/j.ydbio.2003.10.012

552 Wilson MVH, Caldwell MW. 1998. The Furcacaudiformes: A new order of jawless vertebrates with
553 thelodont scales, based on articulated Silurian and Devonian fossils from northern Canada.
554 *Journal of Vertebrate Paleontology* **18**:10–29. doi:10.1080/02724634.1998.10011031

555 Wilson MVH, Caldwell MW. 1993. New Silurian and Devonian fork-tailed "thelodonts" are jawless
556 vertebrates with stomachs and deep bodies. *Nature* **361**:442–444. doi:10.1038/361442a0

557 Yamashita S, Andoh M, Ueno-Kudoh H, Sato T, Miyaki S, Asahara H. 2009. Sox9 directly promotes
558 Bapx1 gene expression to repress Runx2 in chondrocytes. *Experimental Cell Research*
559 **315**:2231–2240. doi:10.1016/j.yexcr.2009.03.008

560 Zeng L, Kempf H, Murtaugh LC, Sato ME, Lassar AB. 2002. Shh establishes an Nkx3.2/Sox9
561 autoregulatory loop that is maintained by BMP signals to induce somitic chondrogenesis. *Genes*
562 *Dev* **16**:1990–2005. doi:10.1101/gad.1008002

563

564

565 **Figures**

566

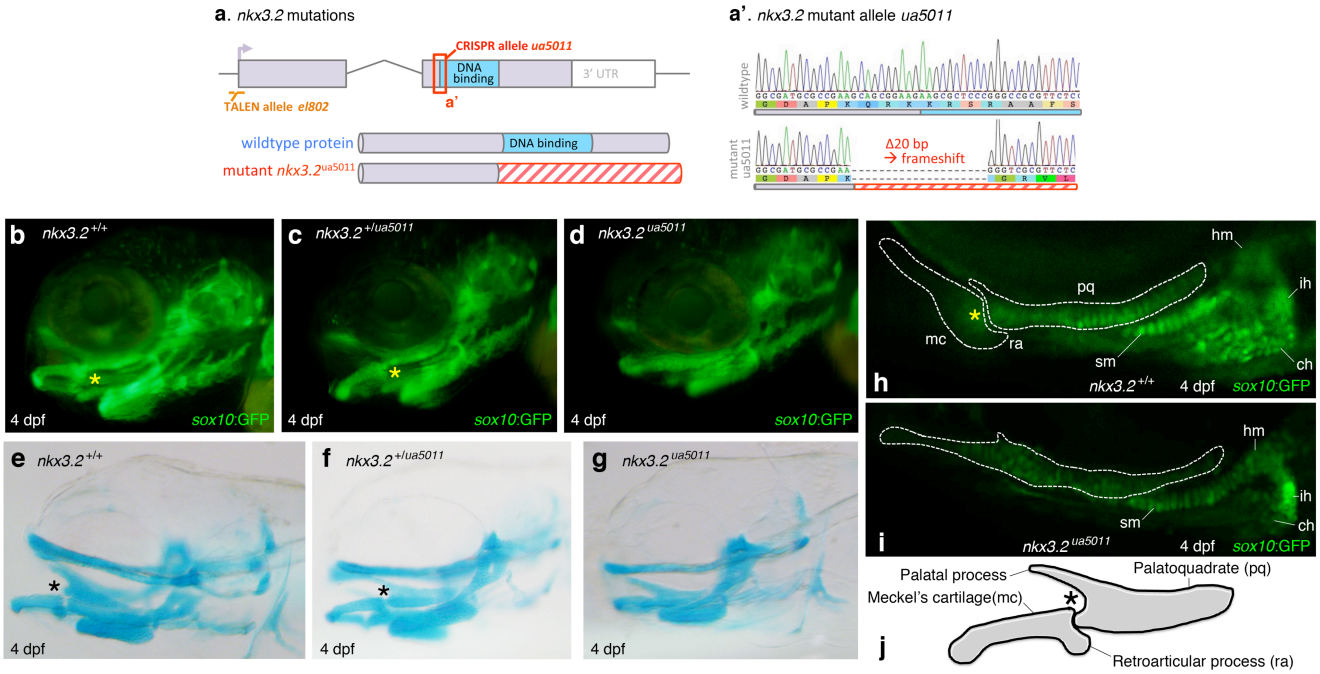

567

568 **Figure 1. Null alleles of *nkx3.2* in zebrafish result in the jaw joint ankylosis.**

569 (**a**) Mutations engineered with CRISPR/Cas9 or TALEN in the zebrafish gene *nkx3.2* that
570 encodes the homeobox transcription factor protein Nkx3.2 (a.k.a. Bapx1). Top: The gene *nkx3.2*
571 contains two exons (purple), the second of which encodes the homeobox domain (DNA binding
572 domain, blue). The diagram is approximately to scale (exon 1 = 310 bp), except the 3' untranslated
573 region (3'UTR). Allele *nkx3.2*^{el802} was generated with TALEN technology that deleted 20 bp from the
574 start of the gene (orange dashed line), eliminating the start codon. Allele *nkx3.2*^{ua5011} was engineered
575 with CRISPR/Cas9 to generate a 20 bp deletion (red box) and frameshift that is predicted to eliminate
576 the homeodomain. Bottom: Schematic of predicted protein following CRISPR mutagenesis. In the
577 allele *nkx3.2*^{ua5011}, the frameshift (20 bp deletion) is predicted to disrupt the translation and abrogate
578 production of the critical homeobox domain. This is predicted to produce random amino acids (red

579 hatching). (**a'**) Sequencing results from allele *nkx3.2*^{ua5011} (lower) compared to a wildtype zebrafish
580 (upper).

581 At 4 dpf, the chondrocrania are compared by *sox10*:eGFP expression in chondrocytes (**b**–**d**, **h**,
582 **i**) or by alcian blue staining of cartilages (**e**–**g**) between age-matched specimens. (**b**, **e**) The
583 chondrocranial morphology of wildtypes (AB background; *sox10*:eGFP) at 4 dpf in left lateral view, in
584 *sox10*:eGFP expression within chondrocytes (b) and alcian blue staining of cartilages (e). (**c**, **f**) The
585 chondrocranial morphology of *nkx3.2* heterozygous mutants (*nkx3.2*$^{+/ua5011}$; *sox10*:eGFP) at 4 dpf in
586 left lateral view, in *sox10*:eGFP expression within chondrocytes (c) and alcian blue staining of
587 cartilages (f). (**d**, **g**) The chondrocranial morphology of *nkx3.2* homozygous mutants (*nkx3.2*^{ua5011};
588 *sox10*:eGFP) at 4 dpf in left lateral view, in *sox10*:eGFP expression within chondrocytes (d) and alcian
589 blue staining of cartilages (g). (**h**, **i**) Comparison of jaw morphology between age-matched wildtype
590 (AB background; *sox10*:eGFP) (h) and *nkx3.2* homozygous mutants (*nkx3.2*^{ua5011}; *sox10*:eGFP) (i) at 4
591 dpf in left lateral view, using *sox10*:eGFP expression within chondrocytes. White broken lines
592 delineate the mandibular cartilages. (**j**) Schematic drawing of the mandibular cartilages in zebrafish at 4
593 dpf in left lateral view, showing wildtype morphology (see panel e).

594 **Abbreviations: asterisk (*)**, jaw joint; **aa**, anguloarticular; **ar**, articular; **bh**, basihyal; **ch**,
595 ceratohyal; **d**, dentary; **dpf**, days post fertilization; **hm**, hyomandibula; **ih**, interhyal; **j**, jugal; **ke**,
596 kinethmoid; **lp**, lower lip; **mc**, Meckel's cartilage; **m**, maxilla; **n**, nostril or aperture of nasohypophyseal
597 system; **o**, operculum; **pm**, premaxilla; **po**, preopercular; **pq**, palatoquadrate; **q**, quadrate; **ra**,
598 retroarticular process; **sm**, symplectic; **up**, upper lip.

599

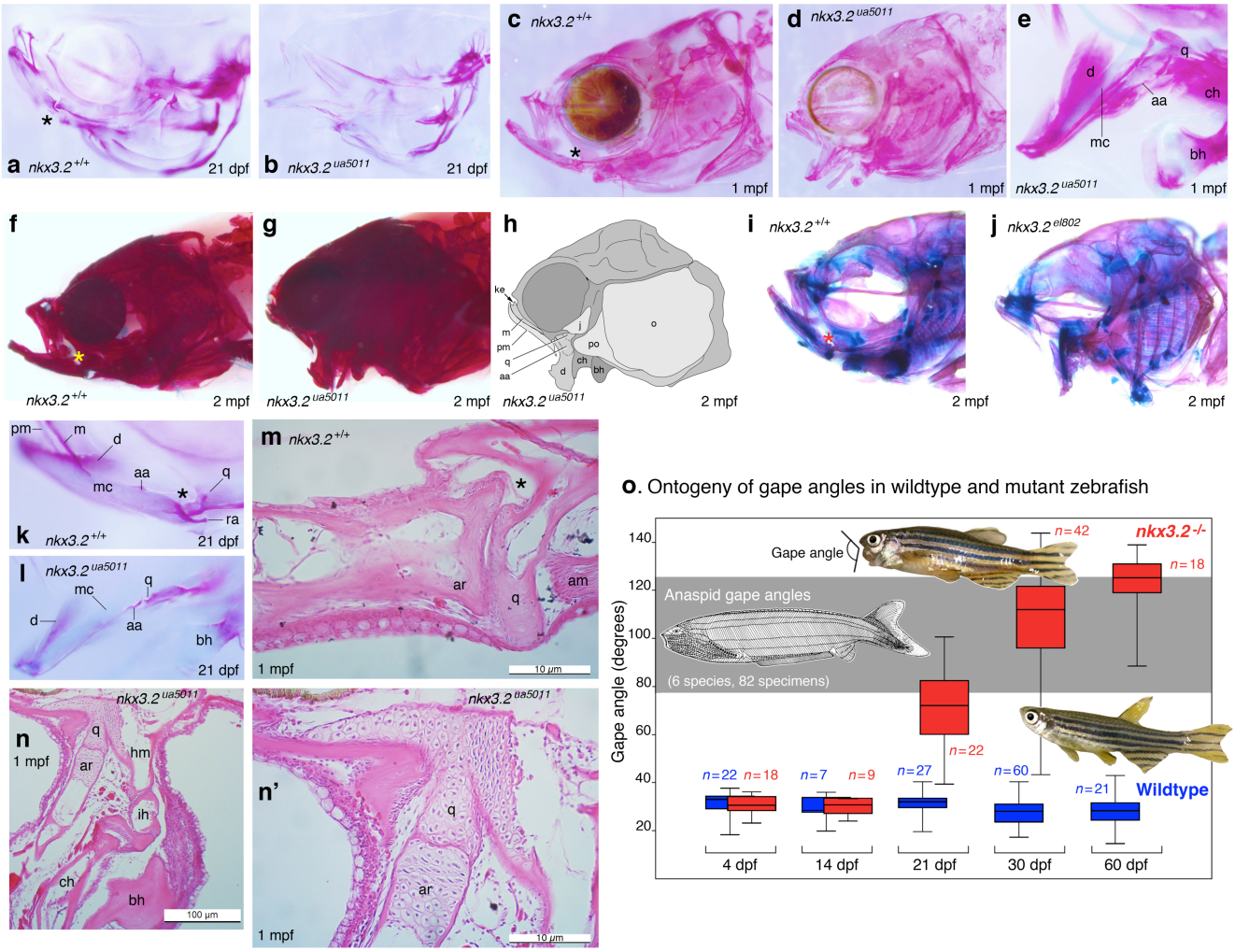

Figure 2. Ontogeny of *nkx3.2*$^{-/-}$ zebrafish documents drastic remodeling of the skull.

(**a**, **b**) Comparison of the skull morphology between age-matched wildtype (AB strain) (a) and *nkx3.2* homozygous mutant (*nkx3.2*^{ua5011}) (b) at 21 dpf in right lateral view (inverted for consistency with other panels), using alcian blue and alizarin red staining. (**c**, **d**) Comparison of skull morphology between age-matched wildtype (AB) (c) and *nkx3.2* homozygous mutant (*nkx3.2*^{ua5011}) (d) at 1mpf in left lateral view, using alcian blue and alizarin red staining. (**e**) Detailed morphology of jaw skeleton in *nkx3.2* homozygous mutant (*nkx3.2*^{ua5011}) at 1 mpf in right lateral view (inverted for consistency with other panels), using alcian blue and alizarin red staining.

609 (**f**, **g**) Comparison of skull morphology between age-matched wildtype (AB) (f) and *nkx3.2*
610 homozygous mutant (*nkx3.2*^{ua5011}) (g) at 2 mpf in left lateral view, using alcian blue and alizarin red
611 staining. (**h**) Interpretive drawing of the specimen in panel g.
612 (**i**, **j**) Comparison of skull morphology between age-matched wildtype (AB) (i) and *nkx3.2*
613 homozygous mutant (*nkx3.2*^{el802}) (j) at 2 mpf in left lateral view, using alcian blue and alizarin red
614 staining. This second independent null allele of *nkx3.2* confirms the phenotypes reported herein.
615 (**k**–**n**) Detailed morphology of jaw joint in wildtype, or the joint-less interface between the
616 upper and lower jaws in *nkx3.2*$^{-/-}$ mutants. (**k**, **l**) Detailed morphology of junction between upper and
617 lower jaws in age-matched wildtype (k) and *nkx3.2* homozygous mutant (*nkx3.2*^{ua5011}) (l) at 21 dpf in
618 left lateral view, using alcian blue and alizarin red staining. (**m**, **n**) Sagittal section of junction between
619 upper and lower jaws in age-matched wildtype (AB) (m) and *nkx3.2* homozygous mutant (*nkx3.2*^{ua5011})
620 (n) at 1 mpf, stained with eosin and hematoxylin. (**n'**) Detailed view of section in panel n.
621 (**o**) Ontogeny of lower jaws in wildtype and *nkx3.2*$^{-/-}$ zebrafish measured here as gape (angle
622 between upper and lower lips). See Data Supplement 2 for original measurements. Values from
623 wildtype and mutant (blue and red) are plotted as boxes of first and third quartile, with middle line
624 displaying mean, and whiskers communicating maximum and minimum values (*n* = sample size).
625 Photographs are male representative specimens at 60 dpf. Grey area indicates range of gape observed in
626 fossil anaspids (see Supplementary Information for details and Data Supplement 2 for original
627 measurements).
628

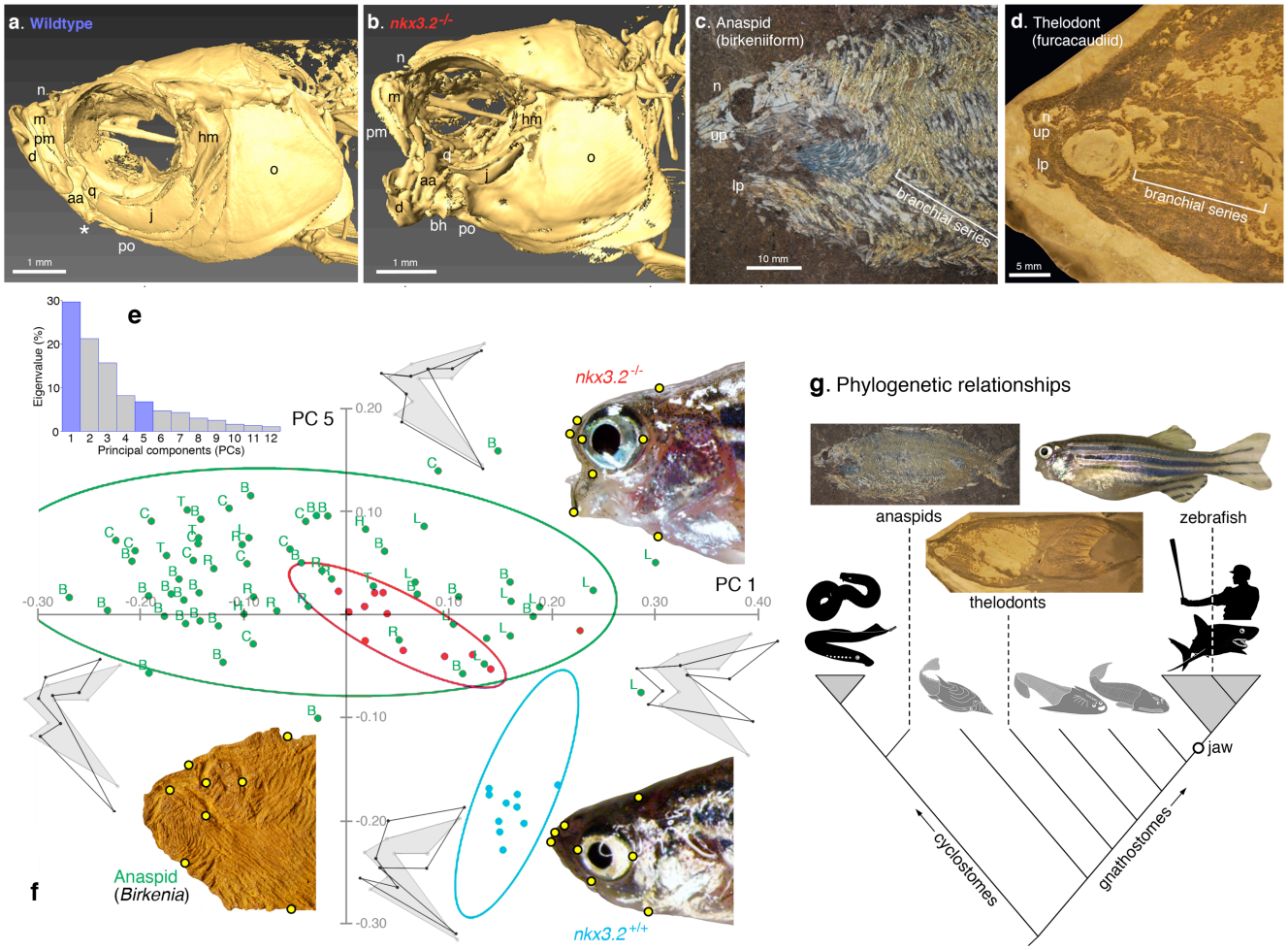

629

630 **Figure 3. Adult *nkx3.2*$^{-/-}$ zebrafish converge onto overall head shapes of anaspids and thelodonts.**

631 (**a**, **b**) Skulls of adult zebrafish in left lateral view via micro-computed tomography (µCT)

632 showing wildtype and *nkx3.2*$^{-/-}$ null mutant zebrafish (allele *ua5011*; 20 bp deletion in homeodomain).

633 The jaw joint is indicated by an asterisk (*) in wildtype (a) and absent in mutant (b). Adult mutants

634 display dramatic phenotypes in the jaw, snout, lips, and orobranchial regions. See also 3D rendering

635 (Movie 1). (**c**, **d**) Skulls of extinct jawless vertebrates, showing general resemblance to the skull shape

636 of *nkx3.2*$^{-/-}$ zebrafish. Morphometric analysis corroborates this similarity. (c) Skull of an anaspid

637 (birkeniid birkeniiform) from the Upper Silurian Cape Philips Formation of Cornwallis Island, Canada

638 (Geological Survey of Canada C-26661-005) in left lateral view. (d) Skull of *Sphenonectris turnerae*, a

639 thelodont (furcacaudiid furcacaudiform) from the Lower Devonian Road River Formation of Northwest

640 Territories, Canada (University of Alberta Laboratory for Vertebrate Palaeontology, specimen number
641 42212).

642 (**e**, **f**) Landmark-based geometric morphometric comparison of *nkx3.2* phenotype using the thin-
643 plate-spline Procrustes superimposition and principal component (PC) analysis. (**e**) Histogram showing
644 loading on each principal component in eigenvalue (%). PCs 1 and 5 are highlighted in blue. These two
645 PCs were chosen for comparison between groups, as these are the two largest components that set apart
646 *nkx3.2* homozygous mutants and wildtype zebrafish from each other at adult stage. PCs 2-4, though
647 accounting for greater variation than PC5, primarily distinguish among anaspids, or within wildtype
648 and mutant zebrafish groups. The original dataset is available (Data Supplement 2). (**f**) A Cartesian plot
649 of PCs 1 and 5, comparing morphospace occupation between wildtypes (2 mpf) (blue), *nkx3.2*
650 homozygous mutants (2 mpf) (red), and anaspids (green), each with 90% ellipse. End of each axis is
651 labeled with a thin-plate-spline shape at that position (dark outline) against mean shape (grey
652 silhouette). A representative specimen is shown with landmarks labeled (yellow circles) for each group
653 in left lateral view. Each data point is a unique biological replicate (a specimen). The anaspid example
654 is *Birkenia elegans*, National Museum of Scotland specimen number 1929.5.6 from a Silurian locality
655 of Scotland. For anaspids, each data point is labeled with taxonomic identifications: B, *Birkenia*
656 *elegans*; C, Birkeniidae indet. from the Cornwallis Island; H, *Pharyngolepis oblongus*; L, *Lasanius*
657 *problematicus*; R, *Ryncholepis parvulus*; T, *Pterygolepis nitidus*.

658 (**g**) Simplified phylogenetic tree of vertebrates to illustrate distant relationships among the taxa
659 compared in this paper. A 60 dpf gravid female specimen is shown for *nkx3.2*$^{-/-}$ zebrafish to capture
660 variations among the mutants (compare with the male in panel e). Photographs of an anaspid and a
661 thelodont are the same individuals in the respective panels showing cranial morphology (d, e). Grey
662 triangle indicates a crown group (not to scale). Dark silhouettes and long branches indicate crown
663 groups, whereas grey silhouettes and short branches represent extinct lineages.

664

Movie

Movie 1. Feeding behaviour and 3D µCT scans of jawless zebrafish. Phenotypic comparison of *nkx3.2*$^{-/-}$ and wildtype zebrafish. Three-dimensional rendering of µCT scan of the age-matched *nkx3.2*$^{-/-}$ (ua5011) and wildtype (AB strain) zebrafish at 2 mpf, each followed by filming of feeding behavior on brine shrimp played at 1/10 original speed.

673 **Supplementary Information**

674

675 **Methods**

676

677 **Zebrafish lines, husbandry, and ethical approvals**

678 Zebrafish maintenance and experiments were approved as protocol number AUP00000077 by the
679 Animal Care and Use Committee: Biosciences at the University of Alberta as dictated by the Canadian
680 Council on Animal Care. Other zebrafish work was approved by the University of Southern California
681 Institutional Animal Care and Use Committee.

682 For *nkx3.2*^{ua5011}, we generated this mutant lineage against AB background. Cas 9 and sgRNAs
683 targeted for *nkx3.2* were coinjected with sgRNA that disrupts GFP GA5'
684 (CTCGGGCTGAAGCTCGGCG), at stages between fertilization and first cleavage, to fertilized eggs
685 collected from the crossing of ua3140 ubi:switch/AB+RH and the background AB line. At 3 dpf,
686 injected larvae were sorted for reduced expression of ubiquitous GFP and the presence of dsRed
687 fluorescence in heart. These larvae provided the P_0 population. Sequencing of genomic DNA extracted
688 from fin clips of the P_0 adults identified a female with a 20 bp deletion to the homeodomain-coding
689 region of *nkx3.2* (ua5011). The P_0 female carrying this mutation was crossed to the *sox10*:GFP
690 transgenic line, and progenies were sorted at 3 dpf for the presence of *sox10*:GFP expression and the
691 absence of the two markers (ubiquitous GFP expression and red fluorescent heart). ua5011
692 heterozygotes were identified by both sequencing of extracted gDNA and RFLP analysis using one
693 XmaI (NEB: R01805) restriction site within the deleted region (primers for genotyping: 5'–
694 GGACGAGACGGATCAGGAATC–3'; 5'–CACTCGGCGTGTTCGGTAAA–3'). These F_1
695 heterozygotes were incrossed for F_2 embryos, which were genotyped by RFLP analysis and phenotyped
696 at 4 dpf by identifying *sox10*:GFP-positive chondrocytes and staining cartilages using alcian blue.
697 Homozygotes were reared with a strictly small-grained diet to the adult stage. In this study,

698 *nkx3.2*$^{ua5011/ua5011}$ represent F_2 generation derived from the P_0 mutant female and a wildtype male (AB;
699 *sox10*:GFP), whereas comparative wildtype (AB; *sox10*:GFP) come from incrossing of half-siblings of
700 the P_0 male.

701 Embryos were incubated at 28 ˚C, and treated with 0.003% PTU (1-phenyl-2-thiourea) in 10%
702 Hank's saline starting at 24 hpf. Larvae were introduced to the nursery at 1 week to 10 dpf. Genomic
703 DNA was extracted from clipped fins of 3-5 dpf larvae or from adults. Preserved tissues, embryos,
704 larvae, and adults were all fixed in 4% PFA, and stored in 100% EtOH or MeOH at -20 ˚C except for
705 adults (preserved in 70% EtOH at 4˚C).

706 For *nkx3.2*^{el802}, TALEN mutagenesis and husbandry protocols followed the previously
707 published description (Barske et al., 2016).

708

709 **Molecular genetics**

710 Nkx3.2 protein is a transcription factor with a homeobox DNA binding domain that is 100% conserved
711 in amino acid sequence among zebrafish, mouse, and human homologs. In zebrafish, a single *nkx3.2*
712 gene is apparent in the genome, and its homology to mammalian *NKX3.2* is strongly supported by gene
713 synteny: e.g. the neighbor genes flanking *nkx3.2* on zebrafish Chromosome 14 (*wdr1* and *bod1l1*) are
714 positioned coordinately in mouse, human and spotted gar.

715 To generate *nkx3.2*^{ua5011}, we designed sgRNA to five different targets near or within the *nkx3.2*
716 homeodomain, which were all injected:

717 GGCGGCCATCTGACGTCGCT

718 GGCTGACGCCAGCAGATCGG

719 AAGCAGCGGAAGAAGCGCTC

720 GAGCGCTTCTTCCGCTGCTT

721 GGCCGCGTTCTCCCACGCGC

722 These targets were selected using the web resource CHOPCHOP (Labun et al., 2016; Montague et al.,

723 2014). Following the protocol developed by Gagnon and colleagues (Gagnon et al., 2014), two
724 different oligonucleotides were ordered: one containing a target sequence led by the SP6 promoter
725 (ATTTAGGTGACACTATA) and followed by the overlapping region
726 (GTTTTAGAGCTAGAAATAGCAAG) of the reverse oligonucleotide; and the reverse containing the
727 constant, Cas9-binding domain of sgRNA. These oliogonucleotides were annealed after 5-minute
728 incubation at 95˚C, through graded cooling (-2˚C s^{-1} to 85˚C; -0.1˚C s^{-1} to 25˚C), and filled in for the
729 non-overlapping regions using T4 DNA polymerase (NEB: M0203S). To synthesize sgRNAs using
730 these templates, MegaScriptTM SP6 Transcription Kit (Ambion: AM1330) was used. The RNAs were
731 precipitated in ammonium acetate solution, suspended in UltraPure™ H_2O, and stored in 2-3 µl
732 aliquots at -80 ℃. For injection, sgRNA(s) were diluted to 400-600 ng μl^{-1}, with 1 µl mixed with 1 µl
733 aliquot of Cas9 nuclease from Streptococcus pyogenes (NEB: #M0646) at 1 µg ml^{-1}. This solution was
734 mixed with 3 µl of 0.2M KCl, 0.2 % phenol red, and ddH_2O. The final injection volume per embryo
735 was approximately 5 nl, with 400-600 pg sgRNA and 1 ng Cas9 nuclease. For control, GFP 5'GA was
736 used at the stage P_0 when ubi:switch/RH+AB was crossed, which can be phenotyped by reduction of
737 ubiquitous GFP in the progenies with dsRed expression in heart.
738

739 **Morphometrics**

740 ***Rationales for the selection of metric traits***. The purpose of our quantitative comparison is to test
741 phenotypic similarities and differences qualitatively identified in *nkx3.2*$^{-/-}$ mutants with respect to
742 wildtype zebrafish and anaspids. On the one hand, the skulls of *nkx3.2*$^{-/-}$ mutants clearly depart from
743 wildtype morphologically at adult stage (Fig. 2). To describe this morphological departure in greater
744 details, we will present comparison of skeletal growth between *nkx3.2*$^{-/-}$ and wildtype elsewhere. On
745 the other hand, it is difficult to assess observed similarities between *nkx3.2*$^{-/-}$ phenotype and the general
746 head configuration in anaspids. Zebrafish and anaspids are distant to each other phylogenetically: the
747 former is nested deep within, in the ascending order, cypriniforms, teleosts, neopterygians,

748 actinopterygians, osteichthyans, and gnathostomes, whereas anaspids represent either a stem
749 gnathostome or even a stem cyclostome lineage (Donoghue et al., 2000; Janvier, 2007, 1996; Keating
750 and Donoghue, 2016; Miyashita et al., 2019). The dermatocranium of a zebrafish is macromeric,
751 although that of an anaspid is largely micromeric with scales of acellular bone (Blom et al., 2001).
752 There is no morphological correspondence in individual elements of the skull roof between zebrafish
753 and anaspids. The parabranchial cavity is closed by the operculum in zebrafish, whereas each branchial
754 pouch had its own outlet in the series of external pores in anaspids (Blom et al., 2001). A single gene
755 mutation in *nkx3.2* did not reverse these, and other morphological differences accumulated after the last
756 common ancestor of zebrafish and anaspids. For morphometric comparison, we chose metric traits that
757 can be identified in both zebrafish and anaspids.
758
759 ***Linear morphometrics***. The fixed open gape is similar between *nkx3.2*$^{-/-}$ mutants and anaspids. We
760 compared this qualitative similarity by taking the angle between supporting skeletal elements of the
761 upper and lower lips in both taxa. In zebrafish, the angle was taken by extrapolating the axis of the
762 premaxilla until it meets the axis of the dentary. At stages younger than the onset of dermal ossification
763 (4 and 14 dpfs), the angle was measured between the axes of the palatal process (palatoquadrate) and
764 Meckel's cartilage. In anaspids, the upper and lower lips are demarcated by a series of plates or
765 relatively larger scales, which allowed delineation of the gape angle.
766 In *nkx3.2*$^{-/-}$ zebrafish, the gape angle increases progressively with age. The timing of lower-lip
767 depression roughly coincides with the onset of dermal ossification. Variation of the gape angle among
768 individuals largely overlaps with that of anaspids (Fig. 2o). However, the increase in gape angle also
769 correlates with an increase in body size, and anaspids have much greater range of body size than
770 zebrafish. Unlike *nkx3.2*$^{-/-}$ zebrafish, the gape angle appears to vary independently of body size in
771 anaspids. No correlation exists between gape angle and orbit diameter in anaspids, regardless of
772 whether among those specimens in the size range of zebrafish or across the entire clade (r = -0.114; P =

773 0.306). Although eye size is generally negatively allometric in vertebrates (Howland et al., 2004), the
774 orbit diameter is one reliable, structurally intact metric trait in this clade, because most specimens are
775 not preserved in entire body length, and because other reference measurements (e.g., body height) are
776 affected by taphonomic deformation or simply not preserved in most specimens (Blom et al., 2001;
777 Blom and Märss, 2010; Janvier, 1996; Sansom et al., 2010).

778 Gape angle exhibits a roughly normal distribution within each of the age class of both *nkx3.2*$^{-/-}$
779 and wildtype zebrafish and among anaspids (see Data Supplement 2). For anaspids, 95% of the
780 variation was calculated. This range is shown in Fig. 2o, independent of age (unknown in anaspid
781 samples) or size (unrelated to variation of gape angles among anaspids). Measurement values are
782 available in Data Supplement 2.

783

784 ***Geometric morphometics***. Eight landmarks were assigned to both zebrafish (2 mpf) and anaspid
785 samples for geometric morphometric comparison (Fig. 3f). These landmarks capture general
786 configuration of the heads (1: anterior tip of upper lip; 2: junction between upper and lower lips; 3:
787 anterior tip of lower lip; 4: nostril, or nasohypophyseal opening; 5: anterior extremity of orbit; 6:
788 posterior extremity of orbit; 7: trunk-head boundary at dorsal outline; 8: ventral point of hypobranchial
789 region). These landmarks describe structures homologous across vertebrates (landmarks 4, 5, 6) or
790 geometrically determined positions comparable across vertebrates. They are free of morphological
791 discontinuity between anaspids and gnathostomes (none of the landmarks represents anaspid- or
792 gnathostome-specific morphology). TpsDig (Rohlf, 2018) was used to place landmarks on two-
793 dimensional images of anaspid and zebrafish. The digitized file was entered into MorphoJ software
794 (Klingenberg, 2011) and all images were aligned using the anterior and posterior extremity of the
795 orbits. These landmark data were transformed using the procrustes superimposition method (Rohlf,
796 1999), and the resulting coordinates were compared using Principal Component Analysis (PCA). In

797 PCA, PC scores from anapsid, *nkx3.2*$^{+/+}$ and *nkx3.2*$^{-/-}$ zebrafish were grouped by equal frequency
798 ellipses with a P value of 0.95.
799
800 ***Rationales for selection of comparative taxa***. Only anaspids were included as a comparative outgroup.
801 There are many other lineages of jawless vertebrates, including living cyclostomes, heterostracans,
802 thelodonts, galeaspids, pituriaspids, and osteostracans, in the order of nested hierarchy toward the
803 crown-group gnathostomes (Janvier, 2007, 1996). Living cyclostomes are difficult to compare as they
804 have an anguilliform profile and lack ossified skeletons, or cartilages unambiguously comparable to the
805 jaw/lip elements of the zebrafish skull (Miyashita, 2016, 2012; Miyashita et al., 2019). Extinct jawless
806 vertebrates generally have a depressiform profile(Janvier, 1996). Therefore, direct shape comparison is
807 difficult with the compressiform zebrafish and anaspids. Among non-depressiform jawless stem
808 gnathostomes, the lips are typically preserved poorly. Furcacaudiform thelodonts have a lateromedially
809 compressed body profile, and have the lip morphology consistent with that of anaspids (Wilson and
810 Caldwell, 1998, 1993). These similarities suggest that depressed lower lips are a general condition
811 along the gnathostome stem, as reconstructed conventionally across the stem group. However, we did
812 not include furcacaudiforms in our morphometric comparison. In furcacaudiforms, the lips are
813 demarcated by numerous scales, which make gape angle difficult to determine (Märss et al., 2007).
814 Landmarks cannot be assigned confidently either. The nasohypophyseal opening cannot be located
815 precisely because of the micromeric nature of the integument on the dorsal side of the head (Wilson
816 and Caldwell, 1998, 1993). The transition from head to trunk is ambiguous along the dorsal outline
817 because there is no apparent change in morphology of the scales (Wilson and Caldwell, 1998, 1993).
818 As such, anaspids remain as the only comparable outgroup taxon to *nkx3.2*$^{-/-}$ mutant zebrafish.
819
820 **Tissue Preparation and Histology**

821 Two-month-old *nkx3.2*$^{+/+}$ and *nkx3.2*$^{-/-}$ zebrafish were fixed in 4% paraformaldehyde for 24hrs.
822 Zebrafish were eviscerated prior to decalcification with 0.5M ethylenediaminetetraacetic acid (EDTA)
823 solution for 4 weeks. Samples were dehydrated post decalcification in a series of graded ethanol and
824 embedded in paraffin. Tissue blocks were embedded in a sagittal orientation and sections were cut at
825 7µm using a 820 Spencer microtome. Hematoxylin and eosin staining was performed on zebrafish
826 sections by firstly placing sections in an oven at 60 °C for 10 min. The deparaffinized sections were
827 rehydrated using xylene and graded ethanol (100%, 95%, 70%), followed by staining with hematoxylin
828 and eosin. The slides were then dehydrated and mounted using Permount.
829

830 **Skeletal preparation**

831 Alcian blue staining of cartilages partly followed the protocol provided by Michael Shapiro (University
832 of Utah). Specimens fixed in 4% PFA were rinsed with ddH_2O and transferred to 70% EtOH. Once
833 equilibrated, larvae were immersed in alcian blue solution (0.167 mg/ml alcian blue; 15% acetic acid;
834 70% EtOH), rinsed through EtOH/ddH_2O series, and washed in a saturated sodium borate solution.
835 Specimens were immersed in trypsin solution (0.125% trypsin; 30% sodium borate) overnight, washed
836 in 1% KOH solution, bleached in 0.15% H_2O_2 0.1% KOH, 25% glycerol solution, immersed through a
837 1% KOH/glycerol graded series into 100% glycerol for storage. Specimens older than 21 dpf were
838 immersed in 0.005% alizarin red solution in 1% KOH overnight, after the first 1% KOH wash and
839 before bleaching in 0.15% H_2O_2 0.1% KOH.
840

841 **Filming**

842 Wildtype (AB; *sox10*:GFP) and *nkx3.2*$^{ua5011/ua5011}$ were filmed at 2 months post fertilization to record
843 feeding behavior (Movie S1). A fish was placed in a 1.4L tank with dark background and given brine
844 shrimp larvae. Feeding was filmed using Canon EOS 760D at 30 frames s^{-1} in dimensions 1280 × 720

845 pixels. The films were cropped and assembled using iMovie (ver. 10.1.9, © 2001-2018 Apple Inc.) and
846 slowed to 1/10 original speed.
847
848 **Imaging**
849 ***Micro- Computed Tomography (µCT).*** 2-month-old zebrafish were scanned using MILabs µCT
850 scanner. Scans were reconstructed at a voxel size of 25µm. Images were analyzed using AVIZO 3-
851 dimensional software (Milabs, Utrecht, Netherlands). 2-Dimensional images used for linear and
852 geometric morphometrics were obtained from AVIZO.
853 ***Microscopy.*** Fluorescent images were acquired on a Zeiss Axio Observer.Z1 with LSM 700 confocal
854 microscope via ZEN 2010 software (version 6.0, Carl Zeiss MicroImaging, Oberkochen). Brightfield
855 imaging of stained preps was performed on a Leica MZ16F dissection microscope (Concord ON,
856 Canada) with 12.8 megapixel digital camera (DP72, Olympus; Richmond Hill ON, Canada).
857
858 **DATA SUPPLEMENTS**
859 **Data supplement 1.** Sequence information for the *nkx3.2* allele ua5011.
860 **Data supplement 2.** Gape angles in zebrafish; gape angles and orbit diameter in anaspids; thin-plate-
861 spline landmark data in zebrafish (wildtype and *nkx3.2*$^{-/-}$) and anaspids used for Procrustes
862 transformation, which were subjected to principal component analysis.
863